

Uranium, thorium and REE partitioning into sulfide liquids: Implications for reduced S-rich bodies

Anke Wohlers*, Bernard J. Wood

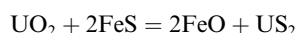
Department of Earth Sciences, University of Oxford, South Parks Road, Oxford OX1 3AN, UK

Received 20 July 2016; accepted in revised form 25 January 2017; available online 24 February 2017

Abstract

We have performed experiments at 1.5 GPa over the temperature range 1400–2100 °C to determine the partitioning of lithophile elements (U, Th, Eu, Sm, Nd, Zr, La, Ce, Yb) between sulfide liquid, low-S metals and silicate melt. The data demonstrate pronounced increases in partitioning of all the lithophile elements into sulfide at very low FeO contents (<1 wt%) of the silicate melt such that $D_U = \left(\frac{[U]_{\text{sulfide}}}{[U]_{\text{silicate}}}\right)$ exceeds 1 and may be >10 in some cases. Similarly D_{Sm} may be >2 under the same conditions of low silicate FeO. This strong partitioning behaviour is found only be important in S-rich metals, however because the observed effect of low FeO on partitioning is uniquely confined to metallic melts close to stoichiometric FeS in composition.

The results and the effects of FeS content of the metal and FeO content (or activity) of the silicate may be understood in terms of exchange reactions such as:



Silicate sulfide silicate sulfide

High concentrations of FeS (in metal) and low FeO contents of the silicate melts drive the reaction to the right, favouring high US_2 in the sulfide and hence high D_U . The effect is, we find, enhanced by the high solubility of S in the silicate (up to 11 wt%) at low FeO contents. This S content greatly reduces the activity coefficient of FeO in the silicate melt, enhancing the displacement of the reaction to the right.

For sulfide-silicate partitioning at 1.5 GPa and 1400 °C we obtain $D_{\text{Nd}}/D_{\text{Sm}}$ of about 1.4 and $D_{\text{Th}} \sim 0.1D_U$. With increasing temperature the differences between these geochemically similar element pairs decreases such that, at 2100 °C $D_{\text{Nd}}/D_{\text{Sm}}$ is 1.0 and D_{Th}/D_U is about 0.3. We used these results, together with D_U and D_{Sm} to model addition of a putative Mercury-like component (with FeS core) to early Earth. We find that the 1400° results could lead to a significant (~11 ppm) ^{142}Nd anomaly in silicate Earth and add >8 ppb U to the core, but lead to an unreasonably high Th/U of silicate Earth (4.54). Based on the 2100 °C results the ^{142}Nd anomaly would be 0 but addition of the sulfur-rich body could add up to 10 ppb of U to the core, generating, when the accompanying 21 ppb Th is also considered, ~3 TW of the energy required for the geodynamo. In this case, the Th/U ratio of silicate Earth would approximate 4.3, within the range of some estimates.

© 2017 The Author(s). Published by Elsevier Ltd. This is an open access article under the CC BY-NC-ND license (<http://creativecommons.org/licenses/by-nc-nd/4.0/>).

Keywords: Sulfide-silicate partitioning; High-pressure experiments; Partitioning behaviour; Lithophile elements; Trace elements

* Corresponding author.

E-mail address: Anke.Wohlers@earth.ox.ac.uk (A. Wohlers).

1. INTRODUCTION

The partition coefficients of many elements between sulfide and silicate liquids follow simple relationships between $\log D_i \left(D_i = \frac{[i]_{\text{sulfide}}}{[i]_{\text{silicate}}} \right)$ and $-\log[\text{FeO}]$ where $[\text{FeO}]$ refers to the FeO content of the silicate melt (Kiseeva and Wood, 2013). One implication of this observation is that even relatively lithophile elements may partition significantly into sulfide at sufficiently low FeO contents of the silicate. This hypothesis was confirmed by Wohlers and Wood (2015) who showed that, under highly reducing conditions (4–6 log f_{O_2} units below the IW buffer) and relatively low temperatures (1400–1650 °C) U, Sm, Nd and other lithophile elements partition strongly into FeS liquids relative to silicate melts. At 1.5 GPa and 1400 °C for example, the partition coefficient for uranium ($D_U = \frac{[U]_{\text{sulfide}}}{[U]_{\text{silicate}}}$) approaches 15 while that for Sm can be greater than 2. The rare earth elements were also found to fractionate quite strongly one from another as they partition between sulfide and silicate liquid with, for example $D_{\text{Nd}}/D_{\text{Sm}}$ of 1.1–1.4 and $D_{\text{Yb}}/D_{\text{Sm}}$ of 0.1–0.6.

Wohlers and Wood (2015) explored the implications of the sulfide-silicate partitioning results by considering the effects on Earth of accretion of a highly reduced sulfur-rich body (similar to Mercury) to the growing planet. They showed that accretion to the Earth of a Mercury-like body having 15–22% by mass of an FeS core and a mantle FeO content of ~0.5 wt% could add 8–10 ppb of U to Earth's core and generate a substantial positive ^{142}Nd anomaly (up to ~17 ppm) in the silicate Earth. Such a “reduced-component” scenario has the potential to address two significant issues in Earth sciences, the energy source for the geodynamo and the apparent “excess” of ^{142}Nd in the mantle. Addition of 8–10 ppb of U to the core would be sufficient to generate about 2 TW, within the 2–5 TW range estimated as being required to generate reasonable core thermal histories (Murthy et al., 2003; Nimmo et al., 2004). Similarly, bulk silicate Earth (BSE) has been found to have higher ratios of radiogenic ^{142}Nd to nonradiogenic ^{144}Nd than the chondritic reference generally regarded as representative of the material from which Earth accreted (Boyet and Carlson, 2005, 2006). ^{142}Nd was produced during the early history of the solar system from decay of extinct ^{146}Sm and the presence of a positive ^{142}Nd anomaly of up to 20 ppm in silicate Earth requires an Sm/Nd ratio higher than chondritic established in the first ~30 Ma of Earth history (Boyet and Carlson, 2005, 2006).

Although Wohlers and Wood (2015) established that U and the REE can partition significantly into FeS liquid at low FeO contents of the silicate melt and that the REE fractionate strongly from one another under these circumstances, their study left a number of major questions still to be answered. Our purpose here was to establish the fundamental chemical behaviour underpinning the observed high sulfide-silicate partition coefficients and to determine the limits of their applicability. The first question to be considered is the role of metal composition. Given that the cores of Mercury, Mars and Earth are all believed to contain significant amounts of S (Nittler et al., 2011; Smith

et al., 2012), determining partitioning behaviour into metals containing S is quite justified. There is, however, no indication that the cores of these planets contain S concentrations close to that of FeS liquid (36.5% S) so it is appropriate to determine the effects of lowering the concentration of S in the metal on the partitioning behaviour of the lithophile elements of interest. We therefore performed a number of experiments in which S/(S + Fe) of the metal was varied from 0 to 0.5 at very low FeO contents of the silicate melt ($\leq 0.5\%$) in order to determine the effect of metal composition on partitioning. Similarly, the experiments demonstrating high partition coefficients into sulfide (Wohlers and Wood, 2015) were performed in the narrow temperature range of 1400–1650 °C and, since the temperatures of differentiation of protoplanetary and precursor bodies are potentially highly variable, it is important to determine temperature effects on lithophile element partitioning. A third question arises from the U-shaped form of the plot of $\log D_i$ versus $\log[\text{FeO}]$ for these lithophile elements. At high FeO contents of the silicate melt the positive correlation between $\log D_i$ and $\log[\text{FeO}]$ arises from the increasing oxygen contents of the sulfide as FeO content of the silicates increases (Wood and Kiseeva, 2015). The lithophile elements simply follow oxygen into the sulfide at these high FeO contents. At low FeO contents, however, we have previously argued that the slope of $\log D_i$ versus $\log[\text{FeO}]$ should converge to the “ideal” value of $-n/2$ where n is the valence of the trace lithophile element of interest (Wood and Kiseeva, 2015). It is clear, however, that D_i is a much stronger apparent function of FeO content at low FeO than is predicted by the simple Kiseeva-Wood model of partitioning. This means that there is a compositional effect on lithophile element partitioning in either the silicate or the sulfide phase which is, as yet unaccounted for. We aimed to determine the reason for this apparently rapid change from weakly to strongly chalcophile behaviour of these lithophile elements at low FeO content. At this stage we believe that pressure effects are of secondary importance to those of temperature and composition and a lack of systematic pressure effects is as shown below, generally confirmed by our study.

2. EXPERIMENTAL AND ANALYTICAL PROCEDURES

Starting compositions and experimental conditions are summarized in Table 1. Major and minor compositions of silicate, sulfide and metal experiments are given in Tables 2–5. Partition coefficients (D) are in Table 6. Experiments were performed at 1.5 GPa and 1635 °C and 2100 °C. Two different, haplobasaltic starting mixtures were used for experiments. For experiments performed at 2100 °C, the starting mixture consisted of ~50 wt% FeS and ~50 wt% of a synthetic silicate close to the 2 GPa eutectic composition of the anorthite-forsterite-quartz system (Liu and Presnall, 1990). At 1635 °C, experiments contained a mixture of 50 wt% of variable mixtures of FeS, Fe and FeSi_2 together with 50 wt% synthetic silicate corresponding to the 1.5 GPa eutectic in anorthite-diopside-forsterite (Presnall et al., 1978). The sulfur-free experiments, were

Table 1

Run conditions and starting material at 1.5 GPa.

Run	Starting composition	<i>T</i> (°C)	Time (min)	Capsule type
663	An ₅₀ Di ₂₈ Fo ₂₂ ^b + 32%FeS + 18%Fe + 2%FeSi ₂	1635	45	Graphite
664	An ₅₀ Di ₂₈ Fo ₂₂ ^b + 32%FeS + 18%Fe + 3%FeSi ₂	1635	45	Graphite
665	An ₅₀ Di ₂₈ Fo ₂₂ ^b + 32%FeS + 18%Fe + 7%FeSi ₂	1635	45	Graphite
666	An ₅₀ Di ₂₈ Fo ₂₂ ^b + 32%FeS + 18%Fe + 8%FeSi ₂	1635	45	Graphite
667	An ₅₀ Di ₂₈ Fo ₂₂ ^b + 32%FeS + 18%Fe + 10.5%FeSi ₂	1635	45	Graphite
699	An ₆₀ Fo ₁₃ Q ₂₇ ^a + 47%FeS + 7%FeSi ₂	2100	10	Graphite
697	An ₆₀ Fo ₁₃ Q ₂₇ ^a + 44%FeS + 12%FeSi ₂	2100	10	Graphite
700	An ₆₀ Fo ₁₃ Q ₂₇ ^a + 39%FeS + 21%FeSi ₃	2100	10	Graphite
701	An ₆₀ Fo ₁₃ Q ₂₇ ^a + 40%FeS + 20%FeO	2100	10	Graphite
706	An ₆₀ Fo ₁₃ Q ₂₇ ^a + 48%Fe + 4%FeSi ₂	1650	30	MgO
702	An ₆₀ Fo ₁₃ Q ₂₇ ^a + 47%Fe + 6%FeSi ₂	1650	30	MgO
703	An ₆₀ Fo ₁₃ Q ₂₇ ^a + 43%Fe + 14%FeSi ₂	1650	30	MgO
704	An ₆₀ Fo ₁₃ Q ₂₇ ^a + 41%Fe + 18%FeSi ₂	1650	30	MgO
681	An ₆₀ Fo ₁₃ Q ₂₇ ^a + 48%Fe + 4%FeSi ₂	1650	60	Graphite
682	An ₆₀ Fo ₁₃ Q ₂₇ ^a + 45%Fe + 10%FeSi ₂	1650	60	Graphite
683	An ₆₀ Fo ₁₃ Q ₂₇ ^a + 47%Fe + 6%FeSi ₂	1650	60	Graphite
684	An ₆₀ Fo ₁₃ Q ₂₇ ^a + 43%Fe + 14%FeSi ₂	1650	60	Graphite
685	An ₆₀ Fo ₁₃ Q ₂₇ ^a + 41%Fe + 18%FeSi ₂	1650	60	Graphite

Experiments were carried out in either graphite or MgO capsules and were doped with a lithophile trace element mix. 1.3% NiS was added to the FeS.

Abbreviations: An (Anorthite), Di (Diopside), Fo (Forsterite), Q (Quartz).

Starting composition after [Presnall et al., 1978^b](#) and [Liu and Presnall, 1990^a](#).

Starting composition proportions are given in wt%.

conducted at 1650 °C, using a mix of ~50 wt% Fe and ~50 wt% of a synthetic silicate of the composition of anorthite-forsterite-quartz ([Liu and Presnall, 1990](#)). Use of the same two silicate compositions as [Wohlers and Wood \(2015\)](#) means that our results are complementary to those of the previous study. Reagent-grade oxides (MgO, SiO₂, Al₂O₃) and carbonate (CaCO₃) were used to separately synthesize anorthite, diopside and forsterite for the starting compositions. For this purpose, the oxides were fired for several hours at 1100 °C before weighing. The fired oxides were mixed with CaCO₃ as the source of calcium and the mixtures decarbonated at 800 °C for ~24 h. The mixtures were then ground, pelletized and fired at 1300 °C for 24 h. A second cycle of grinding and firing was used to ensure homogeneity. The silicate composition was doped with a trace element mix of Zr, La, Ce, Nd, Sm, Eu, Yb, Th and U oxides in proportions yielding concentrations of 1000–2000 ppm. The silicate was mixed with the metal starting material in desired proportions, and ground under acetone for 20 minutes before being dried at 110 °C prior to the experiment. Analytical-grade FeS, Fe and NiS were used for the metal constituent. The FeS was doped with ≤3% NiS in order to provide a second internal standard for trace element analysis of the metal. Appropriate amounts (2–21%) of FeSi₂ or FeO were added to the starting compositions in order to generate silicate melts with low FeO and high FeO content respectively. FeSi₂ is a reductant initially added to reduce the oxidised layer on the powdered FeS starting material. We continued to add FeSi₂ to successive experiments until a second Fe-Si liquid appeared ([Fig. 1a](#)). Experiments were conducted in either 3 mm O.D. and 1 mm I.D. graphite capsules or 6 mm O.D., and 2 mm I.D. MgO capsules.

Experiments were performed in a 1/2-inch diameter piston-cylinder apparatus using an external BaCO₃ sleeve with an SiO₂-glass inner sleeve and graphite furnace of 8 mm O.D. and 6 mm I.D. for experiments at 1635 °C and 1650 °C. The unsealed graphite capsule was separated from the graphite furnace by an MgO spacer which had been fired at 1000 °C to ensure dryness. Fired MgO spacers were employed above and below the capsule with the former having a 1.7 mm hole for the thermocouple. At 2100 °C, the BaCO₃ sleeve was replaced by pyrophyllite and the graphite furnace reduced to 5 mm O.D., 3 mm I.D. The space in between the furnace and silica glass sleeve was filled by a machined polycrystalline MgO cylinder. Temperatures were controlled and monitored by a tungsten-rhenium thermocouple (W₉₅Re₅-W₇₄Re₂₆), and temperature was maintained within ±2 °C. The thermocouple was introduced into the center of the cell, just above the capsule and separated from it by a 0.5 mm alumina disc to prevent puncture of the capsule by the thermocouple. Experiment duration was between 10 min and 2 h. These experimental durations have been found to be sufficient to reach constant partitioning of trace elements in the capsule sizes used in this study ([Tuff et al., 2011](#); [Kiseeva and Wood, 2013](#)). Experiments were quenched by turning off the power supply to the furnace. After quench, the capsule was inspected for cracks and evidence of leaks under a binocular microscope. Complete, unfractured capsules were mounted in acrylic and polished for optical examination and analysis by electron microprobe and Laser Ablation ICPMS.

The experimental conditions, major and trace element compositions of the run products, and the resulting partition coefficients are presented in [Tables 1–6](#).

Table 2
Major element composition of silicate glass.

$P = 1.5$ GPa, $T = 1635$ °C

Run	663		664		665		666		667	
<i>n</i>	62	σ	77	σ	53	σ	84	σ	35	σ
MgO	19.87	0.11	19.71	0.11	18.41	0.18	19.57	0.11	17.75	0.36
Al ₂ O ₃	10.30	0.18	9.38	0.20	8.79	0.09	8.18	0.10	9.99	1.11
SiO ₂	49.11	0.48	49.80	0.94	48.97	0.57	48.95	0.34	49.19	0.50
S	1.59	0.08	3.21	0.08	6.00	0.09	6.78	0.10	7.70	0.10
CaO	17.83	0.15	17.45	0.30	15.86	0.16	14.60	0.16	14.78	0.25
FeO	0.63	0.23	0.55	0.14	0.51	0.18	0.49	0.15	0.45	0.13
Total	99.32		100.10		98.54		98.56		99.87	
log _[FeO]	−0.20		−0.26		−0.29		−0.31		−0.34	

$P = 1.5$ GPa, $T = 2100$ °C

Run	699		697		700		701			
<i>n</i>	38	σ	35	σ	33	σ	50	σ		
MgO	8.53	1.67	5.47	0.04	5.15	0.15	4.86	0.06		
Al ₂ O ₃	15.82	0.85	16.43	0.19	14.61	0.30	13.33	0.16		
SiO ₂	58.16	0.76	60.68	0.29	61.45	0.84	41.37	0.52		
S	6.62	0.17	6.81	0.06	10.78	0.32	0.63	0.16		
CaO	9.81	0.37	9.81	0.07	9.04	0.22	8.38	0.13		
FeO	0.67	0.31	0.63	0.21	0.74	0.10	26.73	0.85		
Total	99.60		99.84		101.78		95.29			
log _[FeO]	−0.18		−0.20		−0.13		1.43			

$P = 1.5$ GPa, $T = 1650$ °C

Run	706		702		703		704			
<i>n</i>	40	σ	40	σ	40	σ	40	σ		
MgO	29.10	8.87	30.91	11.23	29.12	9.94	27.97	6.02		
Al ₂ O ₃	16.10	4.27	15.35	5.85	16.02	4.81	15.91	2.51		
SiO ₂	42.29	0.61	42.22	0.55	42.18	0.65	44.00	0.72		
CaO	9.95	3.17	9.67	4.16	10.17	3.56	9.95	2.08		
FeO	0.48	0.06	0.32	0.06	0.18	0.51	0.13	0.24		
Total	97.92		98.47		97.66		97.96			
log _[FeO]	−0.32		−0.50		−0.76		−0.88			

$P = 1.5$ GPa, $T = 1650$ °C

Run	681		682		683		684		685	
<i>n</i>	57	σ	65	σ	67	σ	50	σ	63	σ
MgO	6.59	0.24	6.43	0.04	6.44	0.05	6.35	0.06	6.30	0.06
Al ₂ O ₃	21.49	0.17	21.30	0.16	21.13	0.21	20.77	0.17	20.73	0.16
SiO ₂	59.01	0.24	59.45	0.23	59.36	0.18	59.07	0.52	58.96	0.33
CaO	11.48	0.10	11.52	0.11	11.56	0.09	11.53	0.23	11.60	0.19
FeO	0.47	0.41	0.30	0.36	0.29	0.25	0.18	0.15	0.15	0.11
Total	99.03		99.00		98.78		97.89		97.74	
log _[FeO]	−0.33		−0.52		−0.53		−0.75		−0.83	

Values in wt%; σ = calculated from error propagation; *n* = number of measurements.

After quenching the experiments, textural observation shows that the initial starting mixtures separated into large sulfide or metal “blobs” of several hundred micron size, which are embedded in a silicate matrix (Fig. 1b, c). The good physical separation between the metallic and silicate liquids enables analysis of both phases using electron microprobe and LA-ICP-MS. The run conditions of all experiments are well above the iron melting temperature and sulfide liquidus conditions determined by Zhang and Hirschmann (2016), which ensures that samples were completely molten during the experiment. In graphite capsules, the silicate liquid quenches to a homogeneous glass (Fig. 1b) while the sulfide melt quenches to a mixture of sul-

fides which, based on microprobe standard deviations (Table 3) are fairly homogeneous on the 10 μ m length scale. The sulfides tend to crack during quenching which leads to the contrasts shown in Fig. 1b. In MgO capsules (Fig. 1c) the silicate quenches to a mixture of glass and elongated quench crystals and includes occasional equant liquidus olivines (Fig. 1c). At low FeO contents in the silicate liquid (<0.5%), two immiscible metallic liquids are present in some S-rich experiments after quench (Table 3), one FeS-rich liquid and a second Fe-Si liquid. An example is shown in the backscattered-electron (BSE) photomicrograph of Fig. 1a, where the central Fe-Si liquid is surrounded by an FeS-rich liquid. The Fe-Si liquid quenches to a homogeneous

Table 3

Major element composition of quenched sulfide liquids and metal liquids.

<i>Sulfide liquids</i>										
<i>P</i> = 1.5 GPa, <i>T</i> = 1635 °C										
Run	663		664 ^a		665 ^a		666 ^a		667 ^a	
<i>n</i>	32	σ	15	σ	39	σ	20	σ	24	σ
O	0.15	0.20	0.07	0.08	0.14	0.18	0.39	0.33	0.18	0.19
Si	0.00	0.01	0.02	0.04	0.02	0.06	0.02	0.03	0.01	0.01
S	29.31	1.19	32.17	2.76	32.83	3.27	32.56	3.20	34.23	1.89
Fe	68.08	1.53	65.30	2.57	64.08	2.70	62.75	3.26	61.69	2.45
Total	97.55		97.56		97.08		95.72		96.10	
<i>P</i> = 1.5 GPa, <i>T</i> = 2100 °C										
Run	699 ^a		697 ^a		700 ^a		701			
<i>n</i>	10	σ	16	σ	19	σ	25	σ		
O	0.01	0.02	0.05	0.13	0.47	0.37	3.91	0.95		
Si	0.01	0.01	0.01	0.02	0.80	0.71	0.08	0.17		
S	35.49	0.68	35.76	0.41	34.50	1.14	28.94	2.05		
Fe	61.99	1.32	61.31	0.72	60.86	0.77	65.44	1.42		
U	n.m.	n.m.	0.02	0.02	0.06	0.06	n.m.	n.m.		
Total	97.49		97.13		97.04		98.38			
<i>Metallic liquids</i>										
<i>P</i> = 1.5 GPa, <i>T</i> = 1650 °C										
Run	706		702		703		704			
<i>n</i>	20	σ	20	σ	20	σ	20	σ		
O	0.00	0.01	0.00	0.02	0.00	0.00	0.00	0.00		
Si	1.79	0.04	3.42	0.05	8.25	0.06	10.94	0.11		
Fe	97.62	0.27	96.58	0.60	90.89	0.26	87.76	0.25		
Total	99.42		100.01		99.14		98.70			
<i>P</i> = 1.5 GPa, <i>T</i> = 1650 °C										
Run	681		682		683		684		685	
<i>n</i>	50	σ	38	σ	41	σ	48	σ	46	σ
O	0.03	0.23	0.09	0.11	0.08	0.07	0.03	0.06	0.01	0.04
Si	2.61	0.36	6.08	0.17	4.32	0.29	9.39	1.22	11.31	0.71
Fe	94.09	0.78	91.89	0.53	93.27	0.75	88.88	4.00	87.54	1.92
Total	96.74		98.06		97.67		98.31		98.86	

Values in wt%; σ = calculated from error propagation; *n* = number of measurements.

a = Sulfide contains small blobs of Fe-Si alloy liquid with extremely low lithophile trace element concentrations.

alloy and was found to have extremely low concentrations of U (1.8 ± 0.96 ppm), Th (0.12 ± 0.04 ppm) and the investigated REE (Zr, La, Ce, Nd, Sm, Eu, and Yb) $< 0.57 \pm 0.48$ ppm.

2.1. Microanalysis

Major element compositions of experimental products were determined using the JEOL 8600 electron microprobe in the Archaeology Department at the University of Oxford. Analyses of silicate glasses and sulfides were determined in wavelength dispersive (WDS) mode using a 15 kV accelerating voltage with a beam current of 20 nA and a defocused 10 μm spot. At least 20 analyses of the silicate and metal phases were performed in each experimental product. Count times for major elements (Si, Al, Ca, Mg, Fe in silicate, Fe in metal) were 30 s on the peak and 15 s on the background. Minor elements (S, Ni, O) were analyzed for 60 s peak and 30 on the seconds background. A range of natural and synthetic standards was used for cali-

bration. Standards for silicate were wollastonite (Si, Ca), jadeite (Al), periclase (Mg) and hematite (Fe). Almandine was used as a secondary standard to check the silicate calibration. Standards for S-bearing metal phases were Ni metal (Ni), galena (S) and hematite (Fe, O). Oxygen in the metallic phase was determined using the Kα peak and an LDE crystal. We determined uranium and samarium contents of 3 product S-rich metals as a check on our Laser Ablation-ICP-MS analyses. In this case we used the Mα peak for U and Lα peak for Sm and employed standards of UO₂ and SmPO₄ respectively and a PET crystal. Operating conditions were 15 kV, 40 nA, and a 10 μm beam. Count time for uranium was 120 s on peak and 60 s background. samarium was analyzed for 150 s on the peak and 75 s background.

Trace elements in silicates and sulfides were measured by Laser Ablation ICPMS employing a NexION 300 quadrupole mass spectrometer coupled to a New Wave Research UP213 Nd:YAG laser at the University of Oxford. A laser repetition rate of 10 Hz and 25–50 μm spot size were used

Table 4
Trace element concentration in silicate glass.

$P = 1.5$ GPa, $T = 1635$ °C

Run	663		664		665		666		667	
<i>n</i>	10	σ	10	σ	10	σ	10	σ	10	σ
Zr90	2795	17	2765	25	2776	45	3115	38	2345	27
La139	1499	10	1488	13	1477	22	1753	22	1306	9
Ce140	7	0.1	7	0.1	9	0.2	6	0.2	6	0.1
Nd142	1167	9	1171	11	1166	17	1368	23	1030	8
Sm152	1840	9	1876	17	1917	27	2233	38	1660	15
Eu153	1602	9	1630	14	1644	31	1919	32	1415	8
Yb174	2130	13	2278	16	2353	16	2781	41	2046	23
Th232	2349	12	2242	18	2486	26	2896	33	2195	28
U238	2257	12	2141	15	2005	54	2200	37	1657	25
Ni60	7	4	11	10	46	22	18	4	49	51

$P = 1.5$ GPa, $T = 2100$ °C

Run	699		697		700		701	
<i>n</i>	6	σ	6	σ	6	σ	5	σ
Zr90	724	9	672	10	649	32	888	14
La139	451	8	525	5	465	16	472	8
Ce140	7	0.4	4	0.1	4	0.5	4	0.5
Nd142	341	6	482	4	351	13	362	3
Sm152	560	11	621	6	585	23	605	5
Eu153	528	14	590	5	543	13	534	7
Yb174	756	15	821	11	751	23	741	7
Th232	815	17	867	8	759	20	778	7
U238	539	12	506	5	527	33	712	11
Ni60	8	7	16	14	25	21	9	5

$P = 1.5$ GPa, $T = 1650$ °C

Run	706		702		703		704	
<i>n</i>	6	σ	6	σ	6	σ	6	σ
Zr90	1272	62	1172	133	1362	9	1262	18
La139	648	29	578	66	635	3	591	10
Ce140	4	0.1	4	0.5	4	0.03	4	0.1
Nd142	505	23	456	54	491	4	458	7
Sm152	800	36	719	82	799	5	752	14
Eu153	715	32	651	74	711	5	673	9
Yb174	922	43	796	90	941	7	878	11
Th232	1011	51	895	102	1018	7	963	21
U238	983	45	900	105	989	10	946	17
Ni60	0.4	0.3	0.4	0.2	0.6	0.1	1	0.05

$P = 1.5$ GPa, $T = 1650$ °C

Run	681		682		683		684		685	
<i>n</i>	6	σ	6	σ	6	σ	6	σ	6	σ
Zr90	1654	9	1588	30	1575	22	1685	254	1560	87
La139	815	5	788	12	752	10	777	117	748	42
Ce140	5	0.1	5	0.1	5	0.1	6	2	5	0.4
Nd142	630	3	614	9	582	7	601	92	579	34
Sm152	1024	4	991	13	945	14	976	147	959	56
Eu153	919	3	896	11	846	14	888	141	855	49
Yb174	1221	7	1172	15	1111	12	1154	175	1135	67
Th232	1300	4	1255	17	1172	16	1241	183	1226	68
U238	1315	8	1276	12	1189	20	1296	201	1227	69
Ni60	2	3	0.9	1.1	0.6	0.2	3	2	2	1

Values in ppm; σ = calculated from error propagation; *n* = number of measurements.

for silicate and sulfide phases with an energy density of ~ 12 J.cm⁻². Operating in time-resolved mode, we employed 20 s of background acquisition, followed by ablation for 60 s. Between analyses we employed a 60–90 s

“wash-out” time. The following masses were counted: ²⁴Mg, ²⁷Al, ²⁹Si, ⁵⁷Fe, ⁶⁰Ni, ⁴³Ca, ⁹⁰Zr, ¹³⁹La, ¹⁴⁰Ce, ¹⁴²Nd, ¹⁵²Sm, ¹⁵³Eu, ¹⁷⁴Yb, ²³²Th, ²³⁸U. Our external standard was NIST610 glass and we typically collected 3 spectra

Table 5

Trace element concentration in quenched sulfide liquids and metal liquids.

<i>Sulfide liquids</i>										
<i>P</i> = 1.5 GPa, <i>T</i> = 1635 °C										
Run	663		664		665		666		667	
<i>n</i>	10	σ	9	σ	9	σ	6	σ	8	σ
Zr90	8	1	49	15	330	34	678	74	566	79
La139	27	3	66	23	242	48	213	78	343	20
Ce140	0.2	0.03	0.4	0.1	2	0.4	1	0.3	2	0.2
Nd142	21	2	52	15	199	35	195	32	292	15
Sm152	27	2	70	20	281	44	332	51	414	24
Eu153	110	12	170	56	412	81	400	80	464	26
Yb174	4	0.5	14	3	60	4	150	79	83	13
Th232	1	0.4	8	2	77	13	80	21	153	9
U238	78	4	242	59	1137	154	1063	182	1717	95
Ni60	15,766	475	15,714	1063	12,694	1063	8683	540	7313	552
<i>P</i> = 1.5 GPa, <i>T</i> = 2100 °C										
Run	699		697		700		701			
<i>n</i>	5	σ	5	σ	10	σ	5	σ		
Zr90	221	24	412	70	800	71	10	3		
La139	91	28	172	29	183	77	5	1		
Ce140	1	0.4	2	0.3	2	1	0	0		
Nd142	80	22	183	27	169	66	4	1		
Sm152	137	35	235	29	278	108	6	2		
Eu153	121	34	128	15	119	61	10	2		
Yb174	127	23	182	36	250	77	4	2		
Th232	102	32	169	30	259	86	4	1		
U238	238	57	477	53	747	165	33	4		
Ni60	2331	415	2383	868	1123	270	2907	112		
<i>Metallic liquids</i>										
<i>P</i> = 1.5 GPa, <i>T</i> = 1650 °C										
Run	706		702		703		704			
<i>n</i>	6	σ	6	σ	6	σ	6	σ		
Zr90	0.08	0.04	0.04	0.05	0.1	0.03	1.4	0.6		
La139	0.06	0.04	0.01	0.01	0.08	0.16	0.07	0.05		
Ce140	0.03	0.03	0.01	0.01	0.04	0.03	0.03	0.01		
Nd142	0.06	0.05	0.05	0.07	0.024	0.018	0.1	0.03		
Sm152	0.10	0.07	0.04	0.05	0.03	0.02	0.1	0.02		
Eu153	0.09	0.06	0.01	0.002	0.08	0.09	0.09	0.05		
Yb174	0.07	0.04	0.03	0.02	0.02	0.01	0.08	0.06		
Th232	0.07	0.03	0.004	0.001	0.01	0.00	0.08	0.06		
U238	0.07	0.03	0.10	0.17	0.2	0.3	0.2	0.1		
Ni60	52	1	52	1	53	0	56	5		
<i>P</i> = 1.5 GPa, <i>T</i> = 1650 °C										
Run	681		682		683		684		685	
<i>n</i>	6	σ	6	σ	6	σ	6	σ	6	σ
Zr90	1.1	1.0	1.4	0.2	1	0.2	2.4	0.2	4	0.2
La139	0.1	0.1	0.1	0.1	0.1	0.1	0.0	0.0	0.2	0.1
Ce140	0.1	0.2	0.1	0.2	0.2	0.2	0.0	0.0	0.1	0.1
Nd142	0.1	0.0	0.1	0.0	0.1	0.1	0.1	0.0	0.2	0.2
Sm152	0.3	0.4	0.1	0.0	0.1	0.0	0.1	0.0	0.2	0.1
Eu153	0.3	0.2	0.3	0.3	0.1	0.1	0.0	0.0	0.3	0.2
Yb174	0.1	0.1	0.0	0.0	0.1	0.0	0.1	0.0	0.1	0.1
Th232	0.1	0.1	0.2	0.4	0.1	0.1	0.0	0.0	0.2	0.1
U238	0.4	0.4	1.3	0.9	1	1	0.6	0.3	3	1
Ni60	99	8	119	12	104	4	64	2	87	37

Values in ppm; σ = calculated from error propagation; *n* = number of measurements.

Table 6
Sulfide-silicate and metal-silicate partitioning coefficients (D).

<i>Sulfide liquids</i>										
<i>P</i> = 1.5 GPa, <i>T</i> = 1635 °C										
Run	663		664		665		666		667	
		σ		σ		σ		σ		σ
Zr90	0.003	0.000	0.018	0.006	0.119	0.012	0.202	0.048	0.241	0.034
La139	0.018	0.002	0.044	0.016	0.164	0.032	0.146	0.078	0.262	0.016
Ce140	0.027	0.005	0.061	0.018	0.203	0.041	0.180	0.072	0.332	0.036
Nd142	0.018	0.002	0.044	0.013	0.171	0.030	0.163	0.060	0.283	0.015
Sm152	0.014	0.001	0.037	0.010	0.147	0.023	0.144	0.016	0.249	0.015
Eu153	0.068	0.008	0.105	0.035	0.251	0.049	0.234	0.078	0.328	0.019
Yb174	0.002	0.000	0.006	0.001	0.025	0.002	0.050	0.028	0.040	0.006
Th232	0.001	0.000	0.003	0.001	0.031	0.005	0.032	0.014	0.070	0.004
U238	0.035	0.002	0.113	0.028	0.567	0.078	0.483	0.168	1.036	0.060
Ni60	2182	1350	1429	1343	275	133	493	127	149	154
<i>P</i> = 1.5 GPa, <i>T</i> = 2100 °C										
Run	699		697		700		701			
		σ		σ		σ		σ		
Zr90	0.304	0.033	0.614	0.105	1.233	0.125	0.011	0.003		
La139	0.202	0.061	0.327	0.056	0.394	0.166	0.010	0.003		
Ce140	0.193	0.059	0.391	0.066	0.500	0.258	0.000	/		
Nd142	0.235	0.066	0.380	0.057	0.481	0.189	0.010	0.003		
Sm152	0.245	0.063	0.379	0.047	0.475	0.186	0.010	0.004		
Eu153	0.229	0.065	0.216	0.025	0.219	0.112	0.019	0.004		
Yb174	0.168	0.030	0.222	0.044	0.333	0.103	0.005	0.002		
Th232	0.125	0.040	0.195	0.035	0.341	0.114	0.005	0.002		
U238	0.441	0.107	0.942	0.106	1.417	0.326	0.046	0.005		
Ni60	286	241	150	146	45	39	323	180		
<i>Metallic liquids</i>										
<i>P</i> = 1.5 GPa, <i>T</i> = 1650 °C										
Run	706		702		703		704			
		σ		σ		σ		σ		
Zr90	0.00006	0.00003	0.00003	0.00004	0.00009	0.00002	0.00114	0.00048		
La139	0.00010	0.00006	0.00002	0.00001	0.00013	0.00025	0.00011	0.00009		
Ce140	0.00697	0.00822	0.00176	0.00190	0.00856	0.00721	0.00661	0.00275		
Nd142	0.00011	0.00010	0.00010	0.00015	0.00005	0.00004	0.00017	0.00006		
Sm152	0.00013	0.00009	0.00005	0.00007	0.00004	0.00002	0.00014	0.00003		
Eu153	0.00012	0.00008	0.00001	0.00000	0.00012	0.00013	0.00013	0.00008		
Yb174	0.00007	0.00004	0.00004	0.00003	0.00003	0.00001	0.00009	0.00007		
Th232	0.00007	0.00003	0.00000	0.00000	0.00001	0.00000	0.00008	0.00007		
U238	0.00007	0.00003	0.00012	0.00019	0.00022	0.00032	0.00020	0.00007		
Ni60	138	97	134	62	94	15	86	10		
<i>P</i> = 1.5 GPa, <i>T</i> = 1650 °C										
Run	681		682		683		684		685	
		σ		σ		σ		σ		σ
Zr90	0.00065	0.00061	0.00087	0.00013	0.00053	0.00011	0.00142	0.00024	0.00276	0.00022
La139	0.00012	0.00013	0.00012	0.00011	0.00009	0.00007	0.00005	0.00001	0.00021	0.00018
Ce140	0.02542	0.03501	0.02866	0.03674	0.03779	0.04584	0.00533	0.00487	0.01773	0.01927
Nd142	0.00014	0.00006	0.00015	0.00007	0.00016	0.00014	0.00010	0.00003	0.00033	0.00036
Sm152	0.00029	0.00036	0.00008	0.00004	0.00008	0.00005	0.00012	0.00005	0.00018	0.00011
Eu153	0.00033	0.00023	0.00031	0.00030	0.00016	0.00010	0.00005	0.00002	0.00034	0.00022
Yb174	0.00007	0.00006	0.00003	0.00001	0.00006	0.00004	0.00005	0.00003	0.00008	0.00005
Th232	0.00007	0.00007	0.00015	0.00029	0.00009	0.00009	0.00002	0.00001	0.00015	0.00010
U238	0.00033	0.00027	0.00102	0.00073	0.00116	0.00112	0.00049	0.00025	0.00205	0.00094
Ni60	48	58	130	153	166	51	23	21	43	29

σ = calculated from error propagation.

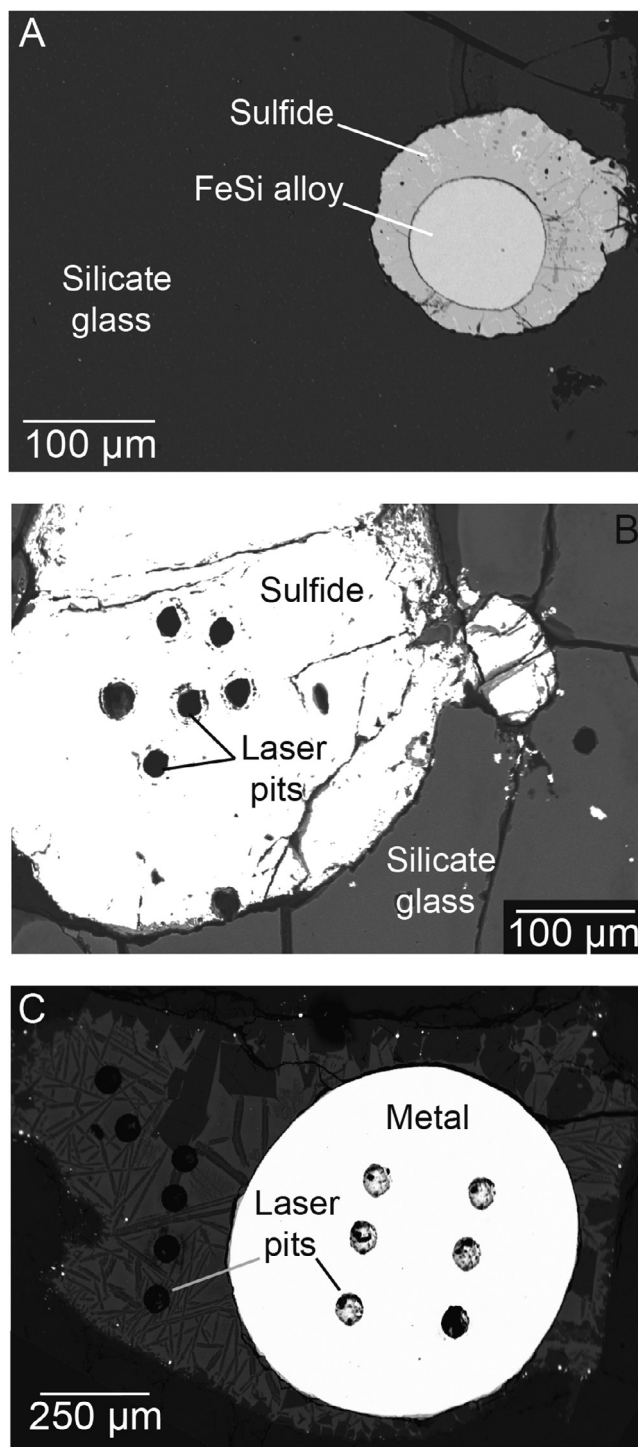


Fig. 1. Backscattered-electron (BSE) photomicrographs of representative experiments at 1.5 GPa. (A) shows an experimental charge (#700) at 2100 °C, where ~21% FeSi_2 was added to the starting mix, yielding a separate Fe-Si-liquid “surrounded by a sulfide rim embedded in homogeneous silicate glass. (B) Experiment #663 at 1635 °C shows a sulfide “blob” in silicate glass. (C) Experiment #702 shows a “blob” of metallic liquid at 1650 °C in silicate glass containing elongated quench crystals.

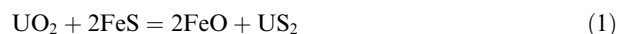
of this at the beginning and end of each sequence of 10–15 unknowns. BCR-2G standard was used as a secondary standard to check the accuracy of the calibration ([supplementary Table 1](#)). Ablation yields were corrected by referencing to the known concentrations of Si and Ca (silicate

glass) and Fe (sulfides and metals), which had been determined by microprobe. Data reduction was performed off-line using the Glitter 4.4.3 software package, which enabled us to identify occasional metal inclusions in the silicate analyses. Since the Fe content of the NIST610 standard is

only 460 ppm, the background is high and the matrices are very different, cross-checks on the sulfide and metal analyses were required. Wohlers and Wood (2015) used Ni as a second internal standard on the microprobe and Laser Ablation ICPMS, and observed no offset in apparent Ni concentration between microprobe and Laser Ablation-ICPMS analyses. Additionally, the U and Sm contents of three experimental quenched liquid sulfides were measured by both electron microprobe and Laser Ablation-ICP-MS (Wohlers and Wood, 2015). Electron microprobe data for the three samples yielded U contents of 3280 ± 490 ppm, 1164 ± 224 ppm and 991 ± 69 ppm, results which are in very good agreement with the Laser Ablation-ICP-MS values of 2960, 951 and 927 ppm respectively. Corresponding microprobe data for Sm are 707 ± 110 ppm, 319 ± 87 ppm and 277 ± 38 ppm, also in excellent agreement with the Laser Ablation-ICPMS results of 719, 326 and 300 ppm respectively. Given this agreement we consider that there should be no systematic bias in our analyses of the S-rich metals for U, Th and the REE.

3. RESULTS

We begin by considering partitioning of trace elements between silicate and a metallic phase which is close in composition to FeS, stoichiometric iron sulfide. Although partitioning of elements between silicate and sulfide depends on the ratio of oxygen fugacity to sulfur fugacity, neither of these variables can be explicitly determined for our experiments. For this reason it is necessary that we redefine partitioning in terms of an exchange reaction with Fe, which simplifies theoretical treatment (Kiseeva and Wood, 2013). In the case of U (IV) the appropriate reaction is:



Silicate sulfide silicate sulfide

The equilibrium constant for reaction (1) may be defined as follows in terms of the activities (a_i) of the 4 components:

$$K_1 = \frac{a_{\text{FeO}}^2 \cdot a_{\text{US}_2}}{a_{\text{FeS}}^2 \cdot a_{\text{UO}_2}} \quad (2)$$

Following Kiseeva and Wood (2013) we assume that the ratio of activity of US_2 to UO_2 is approximately equal to the sulfide-silicate partition coefficient for uranium:

$$D_U = \frac{[\text{U}]_{\text{sulfide}}}{[\text{U}]_{\text{silicate}}} \approx \frac{a_{\text{US}_2}}{a_{\text{UO}_2}} \quad (3)$$

Making this substitution into (2), taking logarithms and assuming that the sulfide is close to pure FeS ($a_{\text{FeS}} = 1$) we obtain, following Kiseeva and Wood (2013):

$$\log D_U \approx A - 2 \log [\text{FeO}] \quad (4)$$

In Eq. (4) constant A is related to the equilibrium constant while $[\text{FeO}]$ refers to the concentration of FeO in the silicate in appropriate units. The important point is that the uranium partition coefficient should increase as the FeO content of the silicate melt decreases. For this reason we plot, in Fig. 2, $\log D_U$ versus the logarithm of the FeO content of the silicate melt in weight percent.

Fig. 2 shows data collected in this study together with those of Wohlers and Wood (2015). As can be seen, and as predicted, D_U is highest at the lowest values of FeO in the silicate melt and decreases with increasing FeO. This trend continues up to FeO concentrations in the silicate of about 3%, then flattens to a minimum and starts to increase with increasing FeO. The increase arises from the increasing oxygen content of the sulfide and the fact that lithophile U tends to follow oxygen (Wood and Kiseeva, 2015) into the sulfide as FeS starts to absorb FeO from the silicate.

Fig. 2 shows that the general features of the plot of $\log D_U$ versus $\log [\text{FeO}]$ described by Wohlers and Wood (2015) apply at all temperatures between 1400 °C and 2100 °C. The temperature effect on uranium partitioning appears to be negligible in this temperature range, the most important feature being that U partition coefficients exceed 10 at the lowest FeO concentrations investigated.

Fig. 3 shows the ratio D_{Th}/D_U for our sulfide-silicate partitioning data. As can be seen, lower temperature data, from experiments at 1400–1650 °C indicate D_{Th}/D_U of the order of 0.1 in the region where D_U is high. Experiments at higher temperature (2100 °C) indicate much stronger partitioning of Th into the sulfide, with D_{Th}/D_U of the order of 0.3 in the low FeO region. This result is important because segregation of sulfide from silicate at low FeO concentration would raise the Th/U of the residual silicate Earth and estimates of the latter place constraints on how plausible and significant the sulfide segregation process may have been in the early Earth. Raising D_{Th}/D_U lowers the impact of sulfide segregation on the Th/U ratio of silicate Earth which means that greater amounts of sulfide removal to the core would be permissible. We deal with quantitative estimates of the effect later in the study.

In order to consider the potential ^{142}Nd anomaly in BSE which would be generated by sulfide segregation to the core under reducing (low FeO) conditions, we require measurements of the sulfide-silicate partition coefficients D_{Sm} and D_{Nd} . Fig. 4 shows the ratio D_U/D_{Sm} measured experimentally. As can be seen, there is excellent consistency between the results at different temperatures and the ratio D_U/D_{Sm} is in the range 2.5–10 in the low FeO region. This means that D_{Sm} values of the order of 1–3 (Table 6 and Wohlers and Wood, 2015) would be plausible under conditions of sulfide segregation at low FeO content of the silicate. Fig. 5 shows the $D_{\text{Nd}}/D_{\text{Sm}}$ ratio for the same experiments. At 1400 °C, D_{Nd} is significantly greater than D_{Sm} with $D_{\text{Nd}}/D_{\text{Sm}}$ ratios commonly in the range 1.3–1.5. As shown by Wohlers and Wood (2015), the greater compatibility of Nd in sulfide relative to Sm has the potential to lead to a ^{142}Nd isotope anomaly in silicate Earth which is of the same order as that proposed by Boyet and Carlson (2005). In distinct contrast, however, are the results at 2100 °C. Under these conditions and in all our high temperature experiments D_{Nd} and D_{Sm} were found to be virtually identical. Thus, the high temperature conditions of high D_{Th}/D_U also correspond to D_{Nd} equal to D_{Sm} .

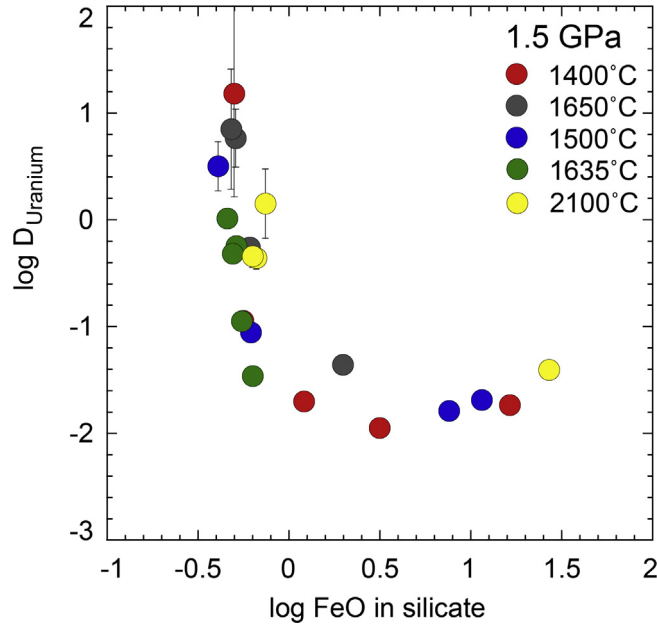


Fig. 2. Sulfide-silicate partitioning coefficients ($D_i = \frac{[i]_{\text{sulf}}}{[i]_{\text{sil}}}$) for uranium plotted versus $\log[\text{FeO}]$ in silicate liquid (wt%) at 1.5 GPa and 1400 °C, 1650 °C and 2100 °C. Data from Wohlers and Wood (2015) and this study. The partition coefficient of U, is, as expected, a strong function of the FeO content of the silicate liquid, increasing dramatically as the FeO content decreases below 1 wt%.

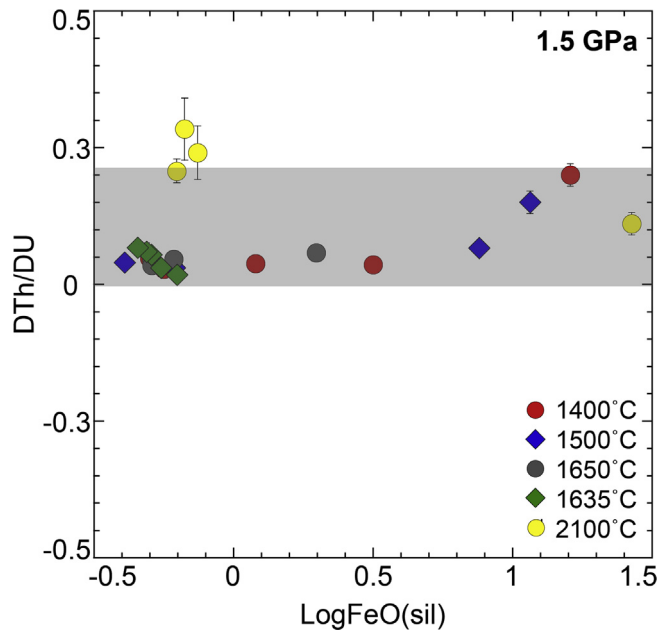


Fig. 3. Sulfide-silicate partition coefficient ratio $D_{\text{Th}}/D_{\text{U}}$ plotted versus $\log[\text{FeO}]$ in silicate liquid at 1.5 GPa and temperatures between 1400 °C and 2100 °C. Data from Wohlers and Wood (2015) and this study. The results show that under reducing conditions ($\text{FeO} < 1$ wt%) and at low temperatures the $D_{\text{Th}}/D_{\text{U}}$ of ~ 0.1 increases to $D_{\text{Th}}/D_{\text{U}} \sim 0.3$ at 2100 °C. This implies that increasing temperature enables Th to more readily accompany U into a sulfur-rich core. Shaded area displays value range.

4. DISCUSSION

4.1. Implications of results for accretion of reduced S-rich bodies to early Earth

Fig. 6 shows 4 illustrative models of U content of the core and ^{142}Nd anomaly of the mantle (relative to bulk

Earth) based on our partitioning data at low temperature (6a,b) and at 2100 °C (6c,d). For these illustrative calculations we assumed that Earth incorporated a reduced body having the same S content as CI chondrite (5.25–6.25%) (Lodders and Fegley, 1998) which translates to 15–21% by mass of FeS depending on whether or not the H and C in CI chondrite had been lost. We took values of D_{Sm}

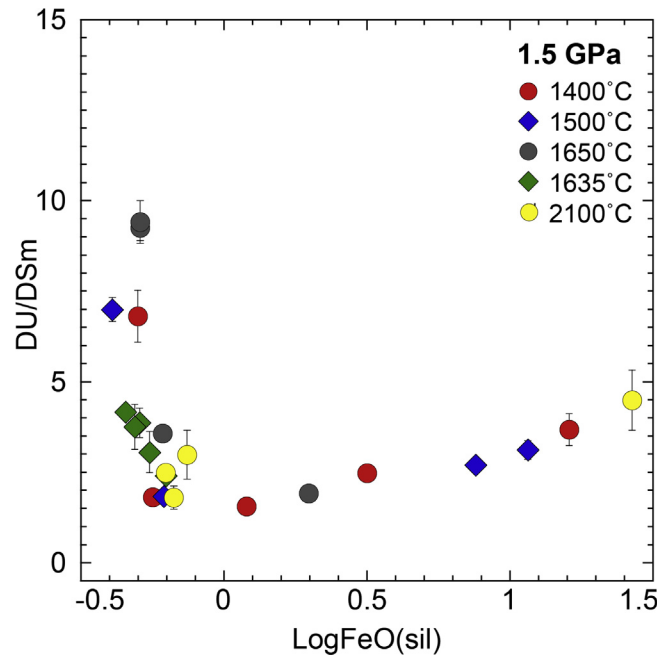


Fig. 4. Shows our measurements of sulfide-silicate partition coefficients for uranium ratio compared to those for samarium. Note that $D_{\text{U}}/D_{\text{Sm}}$ appears to be independent of temperature in the range 1400–2100 °C but that it increases strongly as FeO in the silicate declines below 1 wt%. $D_{\text{U}}/D_{\text{Sm}}$ lies between 2.5 and 10 under low FeO (<1 wt%) conditions.

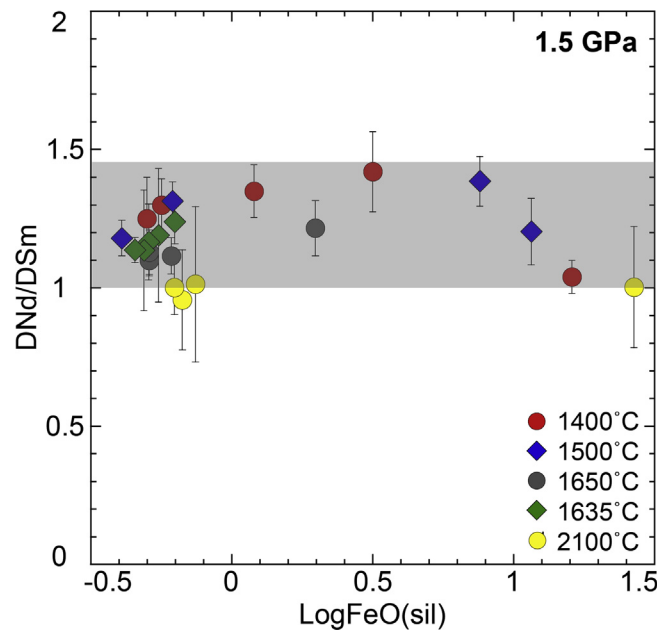


Fig. 5. The partition coefficient ratio $D_{\text{Nd}}/D_{\text{Sm}}$ plotted versus log [FeO] in silicate liquid at 1.5 GPa. Data between 1400 °C and 2100 °C from Wohlers and Wood (2015) and this study. At low temperatures, Nd partitions more strongly into the sulfide than Sm, resulting in $D_{\text{Nd}}/D_{\text{Sm}} = 1.3\text{--}1.5$. The difference between the elements decreases with increasing temperature, however, so that, at 2100 °C $D_{\text{Nd}}/D_{\text{Sm}}$ is approximately 1.

of 1–3, consistent with the highest values we had measured (this study and Wohlers and Wood, 2015) and assumed that the Nd and Sm were added to the FeS core at the beginning of the solar system. The latter assumption yields the largest possible ^{142}Nd anomaly. The ^{142}Nd anomaly was calculated

using a ^{146}Sm half-life and $(^{146}\text{Sm}/^{144}\text{Sm})_{\text{initial}}$ of 68 Myr and 0.0094 respectively (Kinoshita et al., 2012). If we use the alternative values of 103 Myr and 0.0085 (Boyet and Carlson, 2005) then the calculated ^{142}Nd anomaly is 10% lower than that shown. Note that presence of an FeS liquid

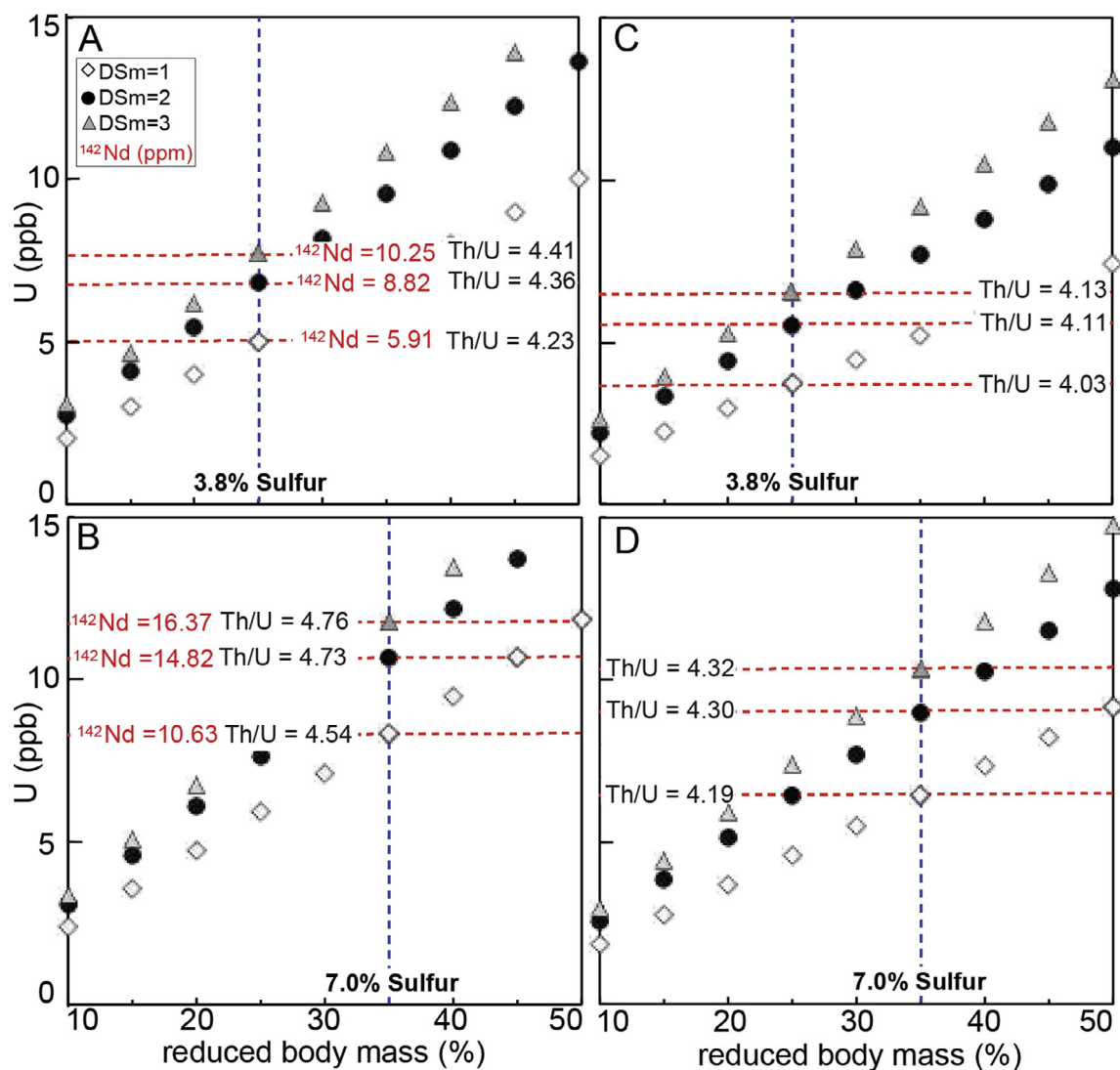


Fig. 6. This figure shows the uranium content (ppb) and the mantle ^{142}Nd anomaly (ppm) predicted from experimental results at low temperature (1400 °C) (6a,b) and at 2100 °C (6c,d). Fig 6a shows the calculated effect of adding a body of 20% Earth mass, containing 0.15 mass fraction sulfide to the growing earth. This yields 3.8 wt% sulfur in the core. $D_{\text{U}}/D_{\text{Sm}}$ was fixed at 5, $D_{\text{Nd}}/D_{\text{Sm}}$ at 1.5 and $D_{\text{Th}}/D_{\text{U}}$ at 0.1, consistent with results at 1400 °C. b) is using the same values as in a), except adding a reduced body of 35% of the Earth mass, with 0.2 mass fraction sulfide, corresponding to 7% S in the core. c) and d) using the same mass fractions of reduced body as in a) and b), but with $D_{\text{U}}/D_{\text{Sm}}$ fixed at 3, $D_{\text{Nd}}/D_{\text{Sm}}$ at 1 and $D_{\text{Th}}/D_{\text{U}}$ of 0.3, consistent with our results at 2100 °C.

core would not, consistent with the experiments discussed above, preclude the presence of an Fe-Si inner core. As can be seen (Fig. 6a), adding 25% of this FeS-rich body to the Earth with a single stage of instantaneous core-merging could, given the low temperature partitioning behaviour lead to 5–8 ppb of U in the core, Th/U of silicate Earth of 4.23–4.41 and a ^{142}Nd anomaly in the mantle relative to bulk Earth of 6–10 ppm. The exact magnitude of the latter in the silicate Earth is subject to discussion, given the possibility of nucleosynthetic effects in meteorite parent bodies and a value of <5 ppm has recently been proposed (Burkhardt et al., 2016). An alternative view (Qin and Carlson, 2016) is of a higher ^{142}Nd anomaly, closer to the original estimate (~20 ppm) even after correction for nucleosynthetic effects. For reference, a ^{142}Nd anomaly of

20 ppm generated at the origin of the solar system corresponds to ($^{147}\text{Sm}/^{144}\text{Nd}$) of 0.209 and a current $\epsilon^{143}\text{Nd}$ of +8.4, within the MORB range (Boyett and Carlson, 2005). Increasing the reduced body mass and sulfide content to 35% of total Earth Mass and 0.20 respectively (Fig. 6b) leads to 8–12 ppb U in the core, Th/U of silicate Earth of 4.54–4.76 and mantle ^{142}Nd anomaly of 11–16 ppm relative to bulk Earth. For reference, a ^{142}Nd anomaly of 20 ppm corresponds to $^{147}\text{Sm}/^{144}\text{Nd}$ of Fig. 6c and d show similar calculations performed using the partition coefficients appropriate for 2100 °C. In this case the virtually identical values of D_{Sm} and D_{Nd} mean that little or no ^{142}Nd anomaly could be present in BSE. On the other hand, considerably greater amounts of U and Th could dissolve in the resultant core with much lower effect on the Th/U ratio

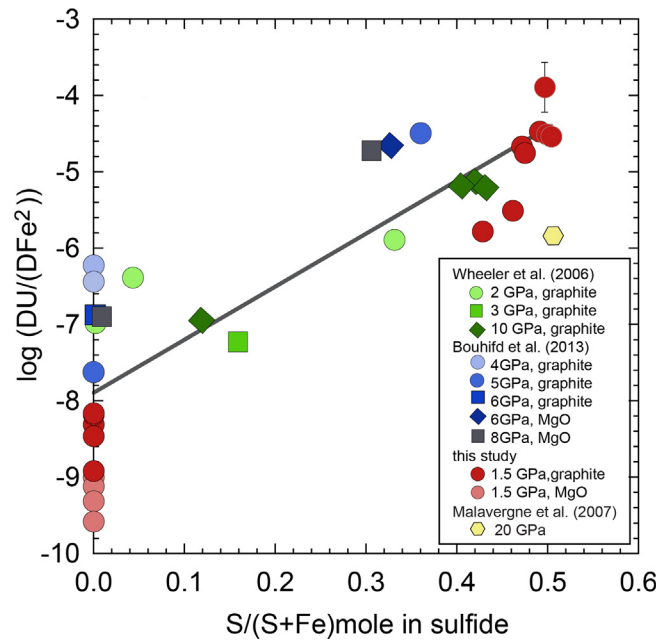


Fig. 7. Plot of $\log(D_U/D_{Fe}^2)$ versus $S/(S + Fe)$ (atomic fraction) in metallic liquid. Data from Wheeler et al., 2006 (2–10 GPa), Bouhifd et al., 2013 (4–8 GPa) (Malavergne et al., 2007) (20 GPa) and this study (1.5 GPa). Note that D_U declines by nearly three orders of magnitude as $S/(S + Fe)$ declines from 0.5 to 0.

of silicate Earth because D_{Th}/D_U is much higher than at 1400 °C. Thus, for example, dissolution of 10 ppb of U in the core would be accompanied by 21 ppb of Th and Th/U of silicate Earth would be 4.3, within the range of some estimates (Tatsumoto, 1978; Allegre et al., 1986). The estimated U and Th contents of the core would lead to 3 TW, sufficient to provide a large proportion of the energy required for the geodynamo (Murrell and Burnett, 1986; Wohlers and Wood, 2015) without taking account of ^{40}K as a potential additional energy source (Murthy et al., 2003; Nimmo et al., 2004). Note that the scenarios shown in Fig. 6 refer to a terrestrial core containing between 3.8 and 7.0 wt% S. The concentration of cosmochemically abundant volatile S in the core is unknown, but recent suggestions range from a cosmochemical estimate of 1.7 wt% (Dreibus and Palme, 1996) to ~6 wt% (Morard et al., 2013) from liquid metal density measurements and 14.7 wt% (Seagle et al., 2006) from high temperature-high pressure equation of state measurements.

4.2. Effect of metal composition on partitioning behaviour

In the previous section, we demonstrated that U, Nd, Sm and other lithophile elements would partition strongly into an FeS-rich planetary core under conditions where the FeO content of the coexisting silicate liquid is very low. This behaviour would have, as shown in Fig. 6, the potential to establish significant concentrations of U and Th in the core and to generate an appreciable ^{142}Nd anomaly in the coexisting silicate mantle. Since S is less abundant in the solar system than Fe, however, and is more volatile than Fe we expect that planetary cores generally have an excess of Fe over S. We therefore wished to consider

whether the strong partitioning of lithophile elements into sulfide also applies to metallic alloys with $Fe/S > 1$.

We performed experiments at 1635 °C and 1.5 GPa (Table 1) in which the FeS was mixed with Fe and FeSi₂ in an attempt to generate silicate melts with low FeO content coexisting with metals of variable $S/(S + Fe)$. Partitioning of all the lithophile elements into the metallic phase was observed to decline rapidly with decreasing S content of the latter. In order to represent the data (Fig. 7), we considered partitioning in terms of an exchange reaction analogous to reaction (1);



silicate metal metal silicate

For which the equilibrium constant is:

$$K_1 = \frac{a_{FeO}^2 \cdot a_U}{a_{Fe}^2 \cdot a_{UO_2}} \quad (6)$$

Equating, as before, activity with concentration this should simplify to:

$$K_4'' \approx \frac{D_U}{D_{Fe}^2} \quad (7)$$

where D_U and D_{Fe} refer to the metal-silicate partition coefficients of U and Fe, respectively.

Fig. 7 shows a plot of $\log K_4''$ versus the $S/(S + Fe)$ ratio of the metal showing our data and those of Wheeler et al. (2006) and Bouhifd et al. (2013). Note that the previous results from pressures of 2–20 GPa, and ours (1.5 GPa) are broadly consistent with one another. We see no systematic effects of pressure on partitioning which indicates that the latter are less important than compositional effects. As can be seen, the partition coefficients for U drop by 3 orders

of magnitude as the S/(S + Fe) decreases from ~0.5 to 0. Similar decreases are observed for D_{Sm} (from 0.48 to 0.01), Nd, Eu, Th and all the other lithophile elements we have investigated here. These observations demonstrate that the strong partitioning of lithophile elements into the metallic phase is confined to metals close in composition to stoichiometric sulfide.

4.3. Effects of FeO concentration on lithophile element partitioning

We turn now to a quantitative explanation for the U-shaped nature of the curve of $\log D_{\text{U}}$ versus $\log[\text{FeO}]$ in Fig. 2. This type of behavior has been observed for a number of strongly lithophile elements including Ti, Ce, Nb and Ta (Wood and Kiseeva, 2015) and U, Sm and Nd (Wohlers and Wood, 2015). From Eq. (4), we anticipate a slope of -2 on our plot of $\log D_{\text{U}}$ versus $\log[\text{FeO}]$. As can be seen from Fig. 2, however the theoretical slope only applies to a small range of FeO contents. The deviations imply that there are strong nonidealities of either sulfide and/or silicate liquids and that these nonidealities are correlated with the FeO content of the silicate melt. We deal with potential nonidealities of sulfide and silicate in turn.

The sulfide liquid in equilibrium with FeO-bearing silicate melt has a certain fraction of its S replaced by oxygen. Kiseeva and Wood (2013, 2015) showed that, at 1.5 GPa and temperatures of 1300 °C to 1500 °C, there is an excellent correlation between the FeO content of the silicate liquid and the oxygen content in the sulfide, empirically expressed as:

$$\text{O (wt\%)} \text{ sulfide} \simeq 0.24\text{FeO (wt\%)} \text{ silicate} \quad (8)$$

Taking account of the differences in atomic weight, this correlation can also be expressed in terms of approximately equal weight percentages of FeO in both phases:

$$[\text{FeO}] \text{ (sulf)} \text{ wt\%} \sim [\text{FeO}] \text{ (silicate)} \text{ wt\%}.$$

Kiseeva and Wood (2015) showed that, as the FeO contents of sulfide and silicate increase beyond 10 wt%, there are increases in the sulfide-silicate partition coefficients of strongly lithophile elements (Mn, Ti, Ce etc) and decreases in the partition coefficients of strongly chalcophile elements such as Ni and Cu. This behavior was attributed to a tendency of lithophile elements to “follow” oxygen into the sulfide and of chalcophile elements to be progressively repelled by the increasing oxygen content of the sulfide. Kiseeva and Wood (2015) parameterized the effect of oxygen in the sulfide on the partitioning between silicate and sulfide by using the epsilon-model of non-ideal interaction in metallic liquids (Wagner, 1962; Ma, 2001). Although not specifically developed for sulfides, Wood and Kiseeva (2015) showed that this simple model reproduces the trace element partitioning with a single “oxygen parameter” in most cases. The principle is that there are interactions between the sulfide component of metal M ($\text{MS}_{n/2}$) and the FeS and FeO components of the sulfide. If these interactions are different, there will be at least one term in the partitioning expression which arises from the differences in activity coefficients of $\text{MS}_{n/2}$ dissolved in FeO-rich and

in FeO-poor sulfide. In the simplest case a single interaction parameter should approximate the observed effect (Wood and Kiseeva, 2015):

$$\log D_{\text{M}} \approx A - \frac{n}{2} \log [\text{FeO}]_{\text{sil}} + \epsilon_{\text{MS}_{n/2}}^{\text{FeO}_{\text{sulf}}} \log(1 - x_{\text{FeO}}^{\text{sulf}}) \quad (9)$$

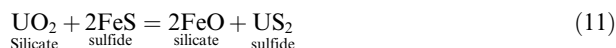
In Eq. (9) the interaction parameter $\epsilon_{\text{MS}_{n/2}}^{\text{FeO}_{\text{sulf}}}$ takes account of the metal-oxygen interaction in the sulfide and $x_{\text{FeO}}^{\text{sulf}}$ to the mole fraction of FeO in the sulfide. We fit the partition coefficient data for U, Sm and Eu in the temperature range from 1400 °C to 1500 °C to Eq. (9) assuming oxidation states of +4, +3 and 2 for U, Sm and Eu respectively. The data for each element were fitted to the equation using the stepwise linear regression model of the SPSS statistic package. Fig. 8 shows that the model of Eq. (9) evolves from the straight line of Eq. (4) to a U-shaped curve and that these 3 elements fit the model reasonably well at high FeO contents. The approach of Eq. (9) does not, however, yield the high partition coefficients at very low FeO conditions ($\log \text{FeO}_{\text{sil}} < 0$) as observed by Wohlers and Wood (2015) and in this study.

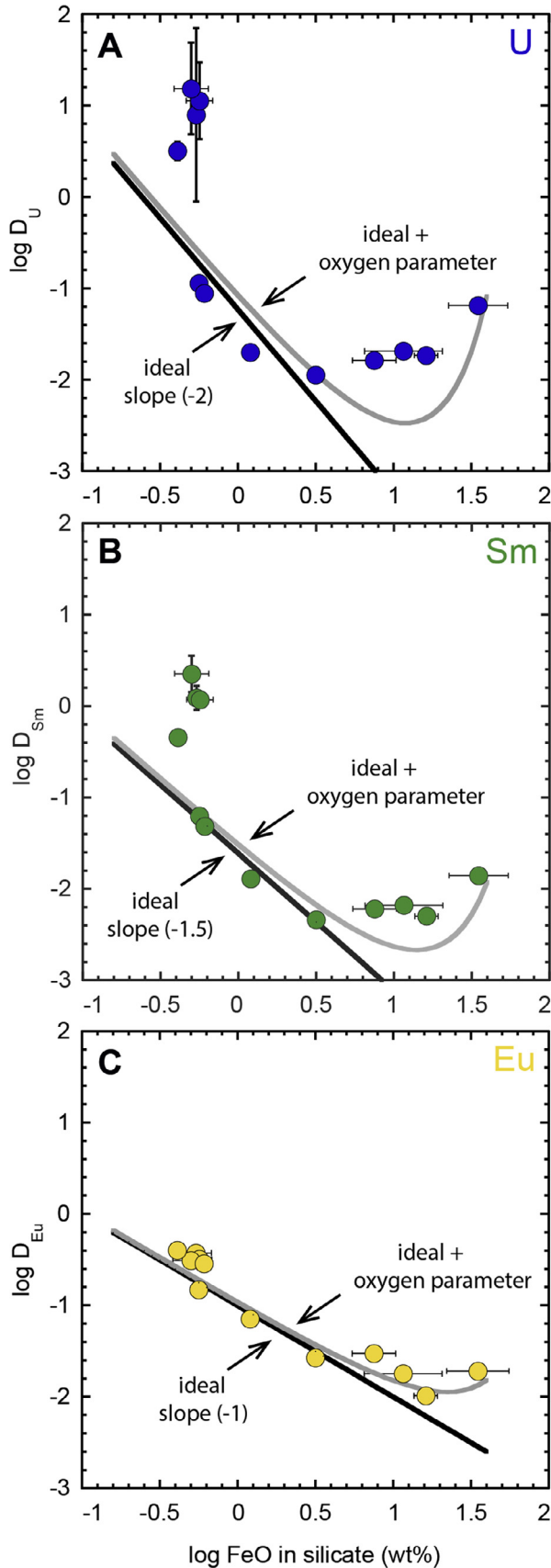
When considering the additional effects which might explain the strong upward curvature in $\log D_{\text{U}}$ at low FeO content, we discounted any effect of the sulfide liquid. This is because the latter only have small excesses of Fe over the “ideal” FeS stoichiometry. The more plausible effect is one involving sulfur in the silicate melt. At low FeO contents (<1 wt%) the S content of the silicate melt rises rapidly, reaching values of ~11 wt% at 2100 °C. Similar dramatic increases in S solubility at low FeO contents and strongly reducing conditions have been observed previously (Kilburn and Wood, 1997; McCoy et al., 1999; Rose-Weston et al., 2009; Zolotov et al., 2013; Malavergne et al., 2014). It is well known that there is a strong interaction between S and FeO dissolved in silicate melt (O'Neill and Mavrogenes, 2002) and we began with the hypothesis that it is this S-FeO interaction which causes the pronounced increases in D_{U} at low FeO and high S concentrations.

O'Neill and Mavrogenes (2002) measured the solubility of sulfur in silicate melt at 1 atm and 1400 °C as a function of the ratio $f_{\text{O}_2}/f_{\text{S}_2}$. They parameterized their results in terms of the compositional dependence of C_{S} , the “sulfide capacity” of the melt as follows:

$$\ln[C_{\text{S}}] = A_0 + \sum_i X_i A_i \quad (10)$$

where A_0 and A_i are constants and X_i are the molecular fractions of the oxide components i in the silicate melt on a single cation basis ie SiO_2 , $\text{AlO}_{1.5}$, FeO etc. The coefficient A_{Fe} was found to be large and positive (+26) for all of the fitting procedures they adopted. As such, the FeO content of the silicate melt has the largest positive influence on sulfur solubility, with the implication being that addition of FeO lowers the activity coefficient of S in the silicate melt. An obvious corollary of this observation should be that high S contents of the silicate melt lower the activity coefficient of FeO. Consider the exchange reaction for U:





Le Chatelier's principle requires that, if we lower the activity of FeO, by lowering its activity coefficient, then the equilibrium will be displaced to the right, favoring entry of U into the sulfide and hence increasing D_U . This is what we observe (Fig. 7). In our original derivation of the dependence of D_U on FeO content, we explicitly assumed that the activity coefficient of FeO is constant, however, enabling us to replace FeO activity by concentration:

$$\log D_U \approx A - 2 \log[\text{FeO}]$$

We therefore need to take account of S-FeO interactions in the silicate melt which act to increase D_i for lithophile elements. This is most readily done by extending the model which we have applied to the sulfide liquid (Eq. (9)) to S-FeO interactions in the silicate liquid. Assuming that the S-FeO term is only significant when FeO is present in the melt in trace quantities, this approach (Ma, 2001) leads to the following expression:

$$\log D_M \approx A - \frac{n}{2} \log [\text{FeO}]_{\text{sil}} + \varepsilon_{MS_{n/2}}^{\text{FeO}_{\text{sulf}}} \log(1 - x_{\text{FeO}}^{\text{sulf}}) + \frac{n}{2} \varepsilon_{\text{FeO}}^{\text{S}_{\text{sil}}} \log(1 - x_{\text{S}}^{\text{sil}}) \quad (12)$$

In Eq. (12) the parameters A , n , $\varepsilon_{MS_{n/2}}^{\text{FeO}_{\text{sulf}}}$ and $x_{\text{FeO}}^{\text{sulf}}$ correspond those in Eq. (9) while $\varepsilon_{\text{FeO}}^{\text{S}_{\text{sil}}}$ refers to the S-FeO interaction parameter for the silicate and $x_{\text{S}}^{\text{sil}}$ to the anion ratio S/(S + O) of the silicate melt. Partition coefficient data for each element were fitted to Eq. (12) using the stepwise linear regression model of the SPSS statistical package by assuming that the REE, except Eu^{2+} are oxidation state +3 and U, Th and Zr are in the +4 state.

As can be seen from Fig. 9, the additional parameter $\varepsilon_{\text{FeO}}^{\text{S}_{\text{sil}}}$ correctly reproduces the strong upward curvature of $\log D_U$ at very low values of $\log[\text{FeO}]$. Our best fit values of $\varepsilon_{\text{FeO}}^{\text{S}_{\text{sil}}}$ are negative and of similar order for all the elements studied except Eu and Ni (Table 7). The agreement is of the correct sign and order to confirm our hypothesis that the upward curvature is due to strong decrease of the FeO activity coefficient as S concentration increases. It implies a decline of γ_{FeO} from just over 1.0 to about 0.05 at the highest S contents of silicate melt measured here. Qualitatively, we would anticipate an increase in apparent $\varepsilon_{\text{FeO}}^{\text{S}_{\text{sil}}}$ with decreasing lithophile and increasing chalcophile nature of the trace element substituent. This is what we observe for Eu^{2+} , a nominally lithophile element which forms the very

Fig. 8. Shows the experimentally determined $\log D_M$ values for U, Sm and Eu as a function of FeO content in silicate liquid. Data from Wohlers and Wood (2015) and this study at 1.5 GPa and temperatures between 1400 °C and 1500 °C. The linear slope (black) shows the predicted behavior of $\log D_M$ with increasing $\log [\text{FeO}]_{\text{sil}}$ (Kiseeva and Wood, 2013). The grey lines correspond to fits to Eq. (9) assuming oxidation states of +4 for U (a), +3 for Sm (b) and +2 for Eu (c). Comparison of measured $\log D_M$ values and predicted fit (Eq. (9)) show that the partitioning of U, Sm and Eu at elevated FeO_{sil} content (>1 wt%) in silicate liquid can be described by the effect of oxygen solubility in sulfide. In contrast at low FeO_{sil} (<1 wt%) the measured D_M values are significantly higher than predicted.

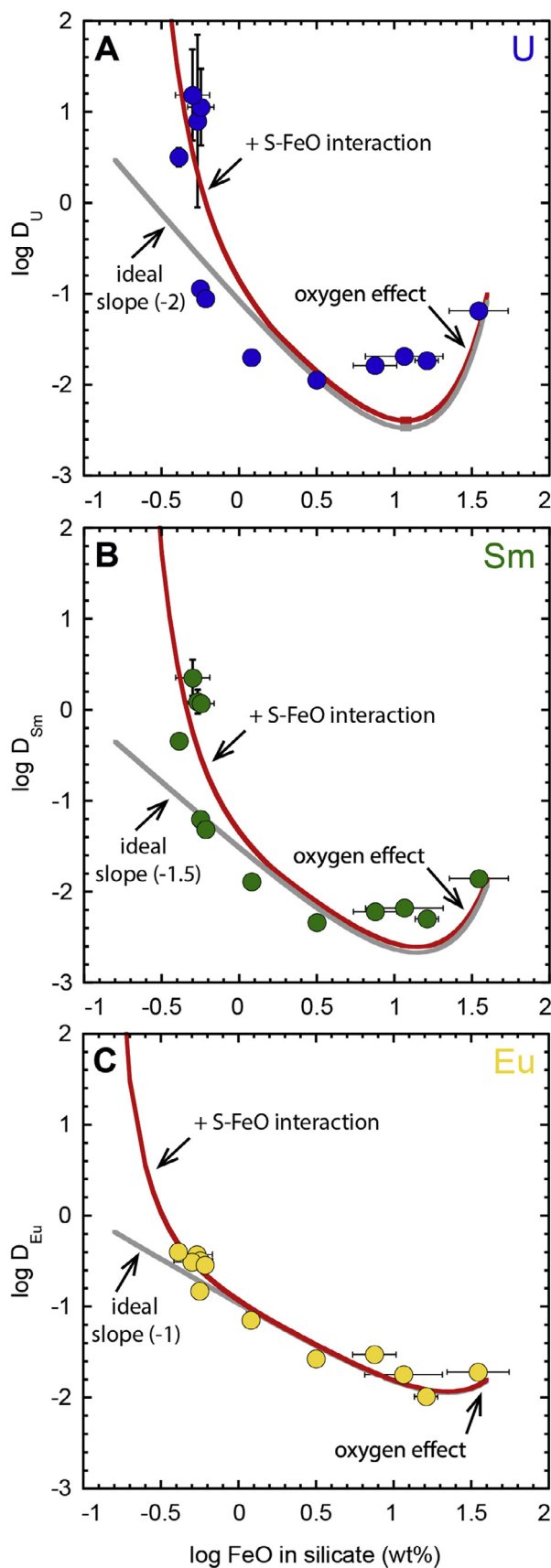


Table 7

Equation parameters for D between sulfide and silicate liquids. $P = 1.5$ GPa, $T = 1400$ °C and 1500 °C

Element	A	σ	$\epsilon_{\text{FeO(sul)}}$	σ	$\epsilon_{\text{S(sil)}}$	σ
U^{+4}	-1.36	0.24	-18.79	2.90	-26.25	5.76
Th^{+4}	-2.79	0.26	-23.28	3.22	-31.50	6.39
Zr^{+4}	-2.76	0.29	-22.74	3.55	-39.56	7.05
Sm^{+3}	-1.66	0.17	-11.35	2.13	-25.59	5.56
Nd^{+3}	-1.51	0.27	-11.13	3.28	-18.85	8.63
La^{+3}	-1.53	0.16	-10.94	1.91	-23.42	5.04
Ce^{+3}	-1.53	0.16	-10.94	1.91	-23.42	5.04
Yb^{+3}	-2.10	0.28	-14.88	3.44	-27.33	9.06
Eu^{+2}	-1.03	0.06	-4.41	0.75	-8.41	2.93
Ni^{+2}	3.11	0.24	-0.34	0.19	42.15	9.07

stable sulfide EuS. Confirmation is provided by the fitted $\epsilon_{\text{FeO}}^{\text{Sul}}$ for Ni^{2+} which is large and of opposite sign to that for all the other elements. This means that, as generally expected, Ni is more chalcophile than Fe and that the activity coefficient of NiO in the silicate decreases more strongly with increasing S than does that of FeO. Thus, counterintuitively, it appears that the more lithophile a trace element the more strongly it partitions into sulfide at low FeO content of the silicate melt. This is because the FeO activity coefficient in the silicate melt decreases with increasing S content of the melt. Conversely, chalcophile elements partition less strongly into the sulfide at low FeO contents because the increasing S content of the silicate melt “pulls” them back into the silicate (Wood and Kiseeva, 2015).

5. CONCLUSIONS

We have confirmed our earlier observations (Wohlers and Wood, 2015) that the lithophile elements U, Sm and Nd partition strongly into sulfide relative to silicate when the FeO concentration in the latter is below 1 wt%. Under conditions of $\text{FeO} < 0.50\%$ D_{U} (sulfide/silicate partition coefficient) approaches 15.3 at 1400 °C and 1.5 GPa while D_{Sm} is ~ 2 . The partition coefficient for uranium, D_{U} and the ratio $D_{\text{U}}/D_{\text{Sm}}$ are relatively insensitive to temperature, at fixed FeO content of the silicate, over the temperature range 1400–2100 °C. In contrast, Th becomes relatively more chalcophile with $D_{\text{Th}}/D_{\text{U}}$ increasing from ~ 0.1 to ~ 0.3 over this temperature interval. Measurements of rare earth element partitioning demonstrate that $D_{\text{Nd}}/D_{\text{Sm}}$ decreases with increasing temperature from ~ 1.4 at 1400 °C and 1.5 GPa to ~ 1.0 at 2100 °C.

Fig. 9. shows $\log D_{\text{M}}$ values for U, Sm and Eu as functions of FeO content of silicate liquid at 1.5 GPa and 1400–1500 °C. The grey curves refer to the fits to Eq. (9), as shown in Fig. 8. The red curves correspond to the calculated fits to Eq. (12). Comparison of measured $\log D_{\text{M}}$ values and predicted fits (Eq. (12)) shows that the partitioning of U, Sm and Eu can be described by considering both the effects of oxygen solubility in sulfide and sulfur solubility in silicate liquid.

The pronounced increase of lithophile element partition coefficients into sulfide at low FeO content is, we believe, most likely due to the coupling between the activity coefficients of S and FeO in the silicate melt. At low FeO concentrations the S contents of the silicate in equilibrium with sulfide liquid rise dramatically with values of ~11 wt% S being reached at FeO concentration of 0.75. Under these conditions the activity coefficient of FeO may decrease from a value of ~1.5 to ~0.05. This effect drives all lithophile elements into the coexisting sulfide, as can be shown from Le Chatelier's principle. We modeled the effect of S on FeO activity by extending the Kiseeva and Wood (2013) model of partitioning into sulfide liquid as follows:

$$\log D_M \approx A - \frac{n}{2} \log [\text{FeO}]_{\text{sil}} + \varepsilon_{\text{MS}_{n/2}}^{\text{FeO}_{\text{sulf}}} \log(1 - x_{\text{FeO}}^{\text{sulf}}) + \frac{n}{2} \varepsilon_{\text{FeO}}^{\text{S}_{\text{sil}}} \log(1 - x_{\text{S}}^{\text{sil}}) \quad (12)$$

Thus, sulfide-silicate partition coefficient D_M (for element M) depends on the FeO content of the silicate [FeO], the valency of the element n and two interaction parameters $\varepsilon_{\text{MS}_{n/2}}^{\text{FeO}_{\text{sulf}}}$ and $\varepsilon_{\text{FeO}}^{\text{S}_{\text{sil}}}$. The former refers to the interaction between M and oxygen in the sulfide and is only significant at FeO contents of the sulfide in excess of 1 wt%. The second parameter $\varepsilon_{\text{FeO}}^{\text{S}_{\text{sil}}}$ refers to the S-FeO interaction parameter for the silicate and $x_{\text{S}}^{\text{sil}}$ to the anion ratio S/(S + O) of the silicate melt. This parameter takes account of the reduction in FeO activity coefficient in the silicate melt as its sulfur content increases.

When these experimental data are considered in the context of a sulfur-rich but highly reduced (low FeO) body with affinities to the planet Mercury, it can be seen that segregation of a sulfide core could generally lead to the core having higher U/Th and Nd/Sm than the mantle. If such a reduced body had been incorporated into Earth early in solar system history it would have left silicate Earth with superchondritic Sm/Nd and Th/U ratios. In such a case the sulfide core of the body would add up to 10 ppb of U to Earth's core, generating, when the accompanying 21 ppb Th is also considered, ~3 TW of the energy required for the geodynamo. In this case, the Th/U ratio of silicate Earth would approximate 4.3. Entry of U and Th into the core would be accompanied by a superchondritic Sm/Nd of silicate Earth, with corresponding small (<14 ppm) excesses of ^{142}Nd occurring provided the sulfide formed in the first few million years of solar system history.

ACKNOWLEDGMENTS

This work was supported by the European Research Council grant number 267764 and the NERC grant NE/N003926/1.

APPENDIX A. SUPPLEMENTARY DATA

Supplementary data associated with this article can be found, in the online version, at <http://dx.doi.org/10.1016/j.gca.2017.01.050>.

REFERENCES

- Allegre C. J., Dupre B. and Lewin E. (1986) Thorium uranium Ratio of the Earth. *Chem. Geol.* **56**, 219–227.
- Bouhifd M. A., Andraut D., Bolfan-Casanova N., Hammouda T. and Devidal J. L. (2013) Metal-silicate partitioning of Pb and U: effects of metal composition on oxygen fugacity. *Geochim. Cosmochim. Acta* **114**, 13–28.
- Boyet M. and Carlson R. W. (2005) ^{142}Nd evidence for early (>4.53Ga) global differentiation of the silicate Earth. *Science* **309**, 576–581.
- Boyet M. and Carlson R. W. (2006) A new geochemical model for the Earth's mantle inferred from (SM)-S-146-Nd-142 systematics. *Earth Planet. Sci. Lett.* **250**, 254–268.
- Burkhardt C., Borg L. E., Brennecka G. A., Shollenberger Q. R., Dauphas N. and Kleine T. (2016) A nucleosynthetic origin for the Earth's anomalous Nd-142 composition. *Nature* **537**, 394–398.
- Dreibus G. and Palme H. (1996) Cosmochemical constraints on the sulfur content in the Earth's core. *Geochim. Cosmochim. Acta* **60**, 1125–1130.
- Kilburn M. R. and Wood B. J. (1997) Metal-silicate partitioning and the incompatibility of S and Si during core formation. *Earth Planet. Sci. Lett.* **152**, 139–148.
- Kinoshita N., Paul M., Kashiv Y., Collon P., Deibel C. M., DiGiovine B., Greene J. P., Henderson D. J., Jiang C. L., Marley S. T., Nakanishi T., Pardo R. C., Rehm K. E., Robertson D., Scott R., Schmitt C., Tang X. D., Vondrasek R. and Yokoyama A. (2012) A Shorter Sm-146 Half-Life Measured and Implications for Sm-146-Nd-142 Chronology in the Solar System. *Science* **335**, 1614–1617.
- Kiseeva E. S. and Wood B. J. (2013) A simple model for chalcophile element partitioning between sulfide and silicate liquids with geochemical applications. *Earth Planet. Sci. Lett.* **383**, 68–81.
- Kiseeva E. S. and Wood B. J. (2015) The effect on the composition and temperature on chalcophile and lithophile element partitioning into magmatic sulfides. *Earth Planet. Sci. Lett.* **424**, 280–294.
- Liu T. C. and Presnall D. C. (1990) Liquidus phase-relationships on the join Anorthite-Forsterite-Quartz at 20 Kbar with applications to basalt petrogenesis and igneous sapphirine. *Contrib. Mineral. Petrol.* **104**, 735–742.
- Lodders K. and Fegley B. J. (1998) *The Planetary Scientist's Companion*. Oxford University Press, Oxford, UK.
- Ma Z. T. (2001) Thermodynamic description for concentrated metallic solutions using interaction parameters. *Metall. Mater. Trans. B* **32**, 87–103.
- Malavergne V., Tarrida M., Combes R., Bureau H., Jones J. H. and Schwandt C. (2007) New high-pressure and high-temperature metal/silicate partitioning of U and Pb: implications for the cores of the Earth and Mars. *Geochim. Cosmochim. Acta* **71**, 2637–2655.
- Malavergne V., Cordier P., Righter K., Brunet F., Zanda B., Addad A., Smith T., Bureau H., Surble S., Raepsaet C., Charon E. and Hewins R. H. (2014) How Mercury can be the most reduced terrestrial planet and still store iron in its mantle. *Earth Planet. Sci. Lett.* **394**, 186–197.
- McCoy T. J., Dickinson T. L. and Lofgren G. E. (1999) Partial melting of the Indarch (EH4) meteorite: a textural, chemical, and phase relations view of melting and melt migration. *Meteorit. Planet. Sci.* **34**, 735–746.
- Morard G., Siebert J., Andraut D., Guignot N., Garbarino G., Guyot F. and Antonangeli D. (2013) The Earth's core composition from high pressure density measurements of liquid iron alloys. *Earth Planet. Sci. Lett.* **373**, 169–178.

- Murrell M. T. and Burnett D. S. (1986) Partitioning of K, U, and Th between sulfide and silicate liquids: implication for radioactive heating of planetary cores. *J. Geophys. Res.* **91**(B8), 8126–8136.
- Murthy V. R., Westrenen W. V. and Fei Y. (2003) Experimental evidence that potassium is a substantial radioactive heat source in planetary cores. *Nature* **423**, 163–165.
- Nimmo F., Price G. D., Brodholt J. and Gubbins D. (2004) The influence of potassium on core and geodynamo evolution. *Geophys. J. Int.* **156**(2), 363–376.
- Nittler L. R., Starr R. D., Weider S. Z., McCoy T. J., Boynot W. V., Ebel D. S., Ernst C. M., Evans L. G., Goldsten J. O., Hamara D. K., Lawrence D. J., McNutt R. L., Schlemm C. E., Solomon S. C. and Sprague A. L. (2011) The major-element composition of Mercury's surface from MESSENGER X-ray spectrometry. *Science* **333**, 1847–1850.
- O'Neill H. S. C. and Mavrogenes J. A. (2002) The sulfide capacity and the sulfur content at sulfide saturation of silicate melts at 1400 degrees C and 1 bar. *J. Petrol.* **43**, 1049–1087.
- Presnall D. C., Dixon S. A., Dixon J. R., Odonnell T. H., Brenner N. L., Schrock R. L. and Dycus D. W. (1978) Liquidus phase relations on join diopside–forsterite–anorthite from 1 am to 20 kbar – their bearing on generation and crystallization of basaltic magma. *Contrib. Mineral. Petrol.* **66**, 203–220.
- Qin L. P. and Carlson R. W. (2016) Nucleosynthetic isotope anomalies and their cosmochemical significance. *Geochem. J.* **50**, 43–65.
- Rose-Weston L., Brenan J. M., Fei Y. W., Secco R. A. and Frost D. J. (2009) Effect of pressure, temperature, and oxygen fugacity on the metal-silicate partitioning of Te, Se, and S: implications for earth differentiation. *Geochim. Cosmochim. Acta* **73**, 4598–4615.
- Seagle C. T., Campbell A. J., Heinz D. L., Shen G. Y. and Prakapenka V. B. (2006) Thermal equation of state of Fe₃S and implications for sulfur in Earth's core. *J. Geophys. Res. Solar Earth* **111**.
- Smith D. E., Zuber M. T., Phillips R. J., Solomon S. C., Hauck S. A., Lemoine F. G., Mazarico E., Neumann E. A., Peale S. J., Margot J. L., Johnson C. L., Torrence M. H., Perry M. E., Rowlands D. D., Goossens S., Head J. W. and Taylor A. H. (2012) Gravity field and internal structure of Mercury from MESSENGER. *Science* **336**, 214–217.
- Tatsumoto M. (1978) Isotopic composition of lead in Oceanic Basalt and its implication to mantle evolution. *Earth Planet. Sci. Lett.* **38**, 63–87.
- Tuff J., Wood B. J. and Wade J. (2011) The effect of Si on metal-silicate partitioning of siderophile elements and implications for the conditions of core formation. *Geochim. Cosmochim. Acta* **75**, 673–690.
- Wagner C. (1962) *Thermodynamics of Alloys*. Addison-Wesley, Reading, MA.
- Wheeler K. T., Walker D., Fei Y., Minarik W. G. and McDonough W. F. (2006) Experimental partitioning of uranium between liquid iron sulfide and liquid silicate: implications for radioactivity in the Earth core. *Geochim. Cosmochim. Acta* **70**, 1537–1547.
- Wohlers A. and Wood B. J. (2015) A Mercury-like component of early Earth yield uranium in the core and high mantle Nd¹⁴². *Nature* **520**, 337–340.
- Wood B. J. and Kiseeva E. S. (2015) The trace element partitioning into sulfide: how lithophile elements become chalcophile and vice versa. *Am. Mineral.* **100**, 2371–2379.
- Zhang Z. and Hirschmann M. (2016) Experimental constraints on mantle sulfide melting up to 8 GPa. *Am. Mineral.* **101**, 181–192.
- Zolotov M. Y., Sprague A. L., Hauck S. A., Nittler L. R., Solomon S. C. and Weider S. Z. (2013) The redox state, FeO content, and origin of sulfur-rich magmas on Mercury. *J. Geophys. Res. Planet.* **118**, 138–146.

Associate editor: Marc Norman